Coexistence of ferromagnetism and charge density waves in monolayer $LaBr_2$

Jun Zhou[1], Zishen Wang,[2] Shijie Wang[1], Yuan Ping Feng[2,3*], Ming Yang[4,†], Lei Shen[5,‡]

[1] *Institute of Materials Research & Engineering, A*STAR (Agency for Science, Technology and Research), 2 Fusionopolis Way, Innovis, Singapore 138634, Singapore*

[2] *Department of Physics, National University of Singapore, Singapore 117551, Singapore*

[3] *Center for Advanced Two-Dimensional Materials (CA2DM), National University of Singapore, Singapore 117546, Singapore*

[4] *Department of Applied Physics, The Hong Kong Polytechnic University, Hung Hom, Kowloon, Hong Kong SAR, China*

[5]*Department of Mechanical Engineering, National University of Singapore, Singapore 117575*

[*]phyfyp@nus.edu.sg

[†]mingyang@polyu.edu.hk

[‡]shenlei@nus.edu.sg

We show for the first time a formation of magnetic interstitial anionic electrons as a novel charge modulation of charge density wave (CDW) in two-dimensional materials. Via combined first-principles calculations, a low-energy effective model and Anderson's superexchange theory, we find that the nonmagnetic metallic T-phase $LaBr_2$ is unstable and undergoes a 2×1 CDW transition to a magnetic T' phase. Concurrently, the delocalized $5d^1$ electrons of La redistribute and accumulate at the interstitial space in the T' phase, forming anionic electrons. The strong localized nature of the anionic electrons promotes a Mott insulating state and a full spin-polarization, while the overlap of their extended tails yields ferromagnetic direct exchange coupling between them. Such transition introduces a new magnetic form of CDW and its practical tunability, providing exciting possibilities for novel spintronics applications.

A charge density wave (CDW) is a widely observed quantum ordering phenomenon in crystals below a critical temperature, which features real-space periodic lattice distortions and charge density modulation as well as reciprocal-space band gap opening (coined as a CDW gap). [1] The CDW can change a material's properties profoundly and may compete with other quantum ordering phenomena in the same system, attracting tremendous research interest. [2-5] One well-known example is the competition between CDW and magnetism. This is because that CDW gaps decrease the density of states (DOS) at the Fermi level (E_f), while the Stoner criterion for a spontaneous spin polarization requires a high DOS at E_f, thus their coexistence is rare. [6,7] Their mutual suppression has been used to explain the discrepancies on the existence of the magnetism in some two-dimensional (2D) materials. [8-10]

The CDWs in metallic octahedral (T-phase) transition metal dichalcogenides (TMDs) are of particular interest for their wide existence, varied patterns and tunability by external stimuli. [11-16] Interestingly, both the CDW pattern and the underlying mechanism depend critically on the *d*-electron count of the transition metal (TM) ion. The $\sqrt{13} \times \sqrt{13}$ (David star), 2×1 (zigzag-chain) and 2×2 (diamond-chain) clustering of metal ions are most common CDWs for the TMDs with d^1, d^2 and d^3 TM ions, respectively. [11] Correspondingly, while Fermi surface nesting and electron phonon coupling play an important role on the structural instability of d^1 TMDs, the real-space local chemical bonding between the TM ions is responsible for the formation of CDWs in d^2 and d^3 TMDs. [11,17-19] It is noted that this is an overall trend and deviants and other CDW patterns are also possible under certain conditions. For

example, $MoTe_2$ follows the CDW pattern with d^2 TM, however, the Fermi surface nesting picture is also proposed in this material. [20]

On the other hand, electrides, in which excess electrons act as anions (named as anionic electrons), are attracting increasing interest as the spatial ion–electron separation induces exotic physical and chemical properties as well as exceptional applications. [21-25]. The recent two exciting developments of this field are the anionic electrons (AEs) as magnetic centers [26-29] and monolayer electrides (coined as electrenes) [30-34]. In particular, the anionic electrons in magnetic electrenes were shown to possess unique dual localized and extended nature, which have further led to increased interest in such materials. [35-37] The emergence of anionic electrons was explained by a mechanism based on Pauli expulsion, in which valence electrons are "squeezed out" by core electrons when the interatomic distance is sufficiently small. [38-40] For the electrides with relatively large interatomic distances, the metal ions form multicenter chemical bonds, and their excess electrons are confined at the center of their clustered "cages". [38] While the periodic charge modulation in conventional CDWs occurs by changing the occupancy of atomic orbitals, the existence of electrides demonstrates the feasibility of localized electrons at interstitial sites of a material without occupying any atomic orbital. However, a coexistence of CDW, electride and magnetism in 2D materials has not been reported to the best of our knowledge. Thus, it is interesting to explore the possibility of forming anionic electrons as a special form of charge density modulation of CDW.

In this letter, we report the CDW induced magnetic electride state in T-phase $LaBr_2$

monolayer, which demonstrates different behaviors from the T-phase TMDs. i). The La ions in $LaBr_2$ have formal d^1 configuration but it forms a 2×1 CDW, rather than the conventional David star as in TMDs; ii). The 2×1 CDW lattice distortions do not open gaps at E_f but increase the density of states at Fermi energy due to the formation of isolated anionic electron bands. Such high DOS leads to a spontaneous spin splitting, resulting in a coexistence of CDW and magnetism. Besides, we provide a clear physical picture on the formation of magnetic electride states in T'-$LaBr_2$. Our results not only unravel a novel magnetic ordering for the spintronic applications, but also are appealing for multi-functional phase transitions.

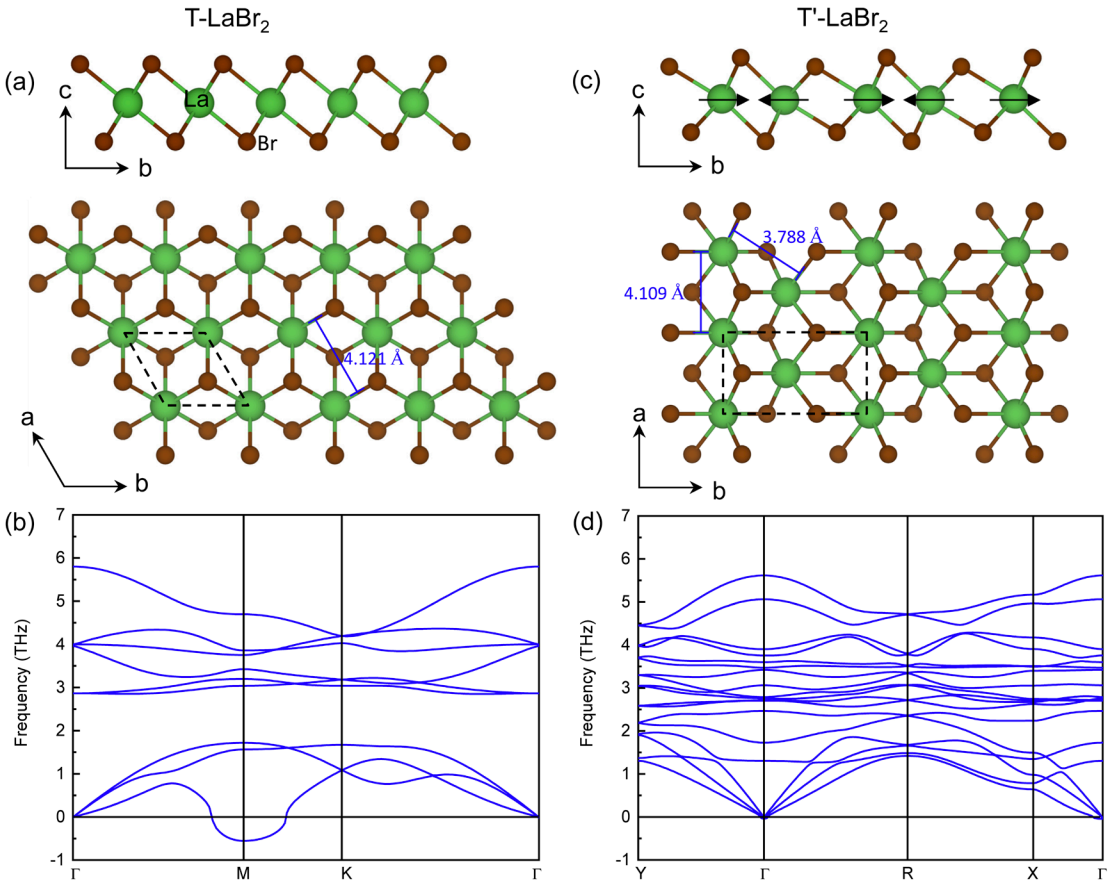

FIG. 1. Side and top view of $LaBr_2$ in (a) T and (c) T' phase structure (visualized by VESTA[41]). The dashed diamond and rectangle in (a) and (c) denote the unit cell of the T and T' $LaBr_2$, respectively. The arrows in (c) indicate the direction of the distortions of La atoms in the T' $LaBr_2$ with T phase as reference.

Phonon band structure of (b) T and (d) T' $LaBr_2$.

The optimized structure of T-phase $LaBr_2$ is shown in **Figs. 1(a)**, which has lattice parameters of $a = b = 4.121$ Å. It contains three atomic layers with La atoms in the middle layer octahedrally coordinated with the top and bottom Br atoms (space group of $P\bar{3}m1$). However, this phase is subject to dynamical instability as suggested by the noticeable imaginary phonon modes shown in **Fig. 1(b)**. The minimum imaginary frequency locates at the high-symmetry point **M**, corresponding to a CDW vector of $\boldsymbol{q} = \boldsymbol{\Gamma M}$, which indicates real-space 2×1 CDW distortions along one of its in-plane lattice vectors. It is noted that similar spontaneous period-doubling distortions have been reported in T-phase group-VI TMDs. [12] However, one important difference between them is the *d* electron count of the metal ions, that is, d^1 of La in $LaBr_2$ while d^2 of TM ions in group-VI TMDs, and the typical CDW of the d^1 group V TMDs is the so-called $\sqrt{13} \times \sqrt{13}$ David Star structure, in contrast with the 2×1 CDW distortions reported here. Such a difference suggests the existing picture of the lattice instabilities for TMDs is unlikely in T-phase $LaBr_2$.

Suggested by the CDW vector of the T-phase $LaBr_2$, a 2×1 supercell structure (T' phase) is constructed. The optimized structure of the T' $LaBr_2$ (space group $P2_1/m$) is shown in **Fig. 1(c)**. It can be obtained by moving every pair of La ions closer to each other along the *b* axis, as indicated by the arrows shown in **Fig. 1(c),** leading to a dimerized structure. The lattice parameters of T' structure are $a = 4.109$ Å and $b = 7.428$ Å. Compared with the high-symmetry T phase, the lattice of the T' structure shrinks along the *a* axis and expands along the *b* axis. The distance between the dimerized La atoms

decreases from 4.121 Å in T phase to 3.788 Å along the *b* axis, suggesting bond formation between the La atoms. With the 2×1 distortions, the T' phase is dynamically stable as the imaginary phonon modes at **M** point vanished and only negligible imaginary phonon frequencies are found around the **Γ** point [see **Fig. 1(d)**]. [42] The total energy of T' $LaBr_2$ is 37.86 meV per formula unit (f.u.) lower than that of the T phase.

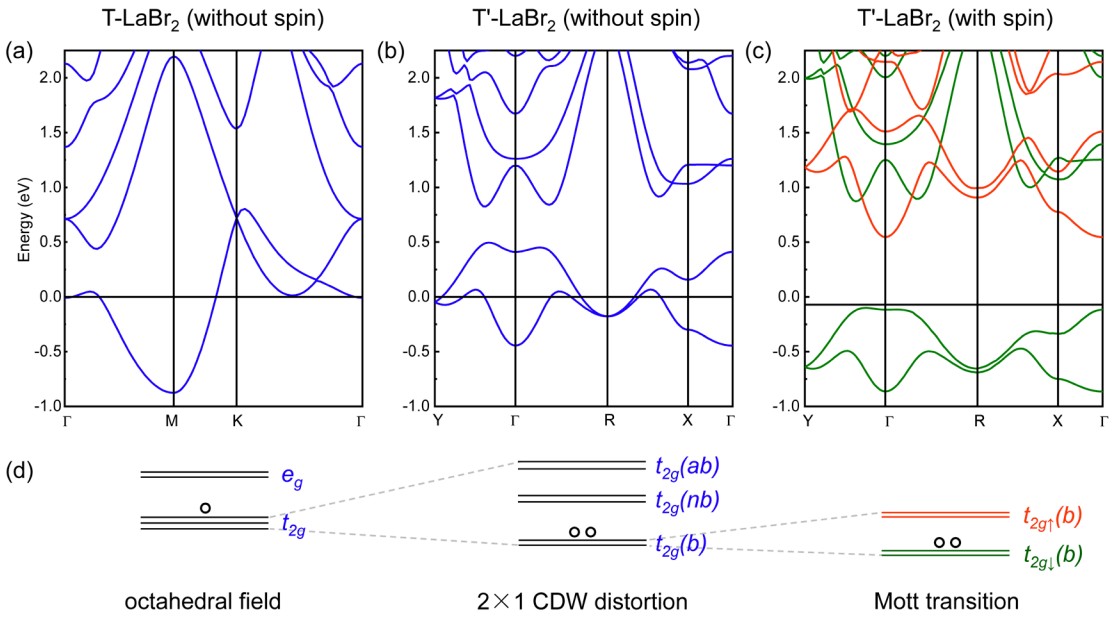

FIG. 2. (a) Band structure of T $LaBr_2$. It is noted that T $LaBr_2$ remains nonmagnetic when spin polarization is switched on in the simulation. Band structure of T' $LaBr_2$ (b) without and (c) with spin polarization. The red and green curves in (c) represent the spin up and spin down bands, respectively. The Fermi level is aligned to 0 eV. (d) Schematic energy level diagrams of transition from T to T' $LaBr_2$.

The band structures of the T and T' $LaBr_2$ are shown in **Figs. 2(a)** to **(c).** The T phase is nonmagnetic and metallic [see **Fig. 2(a)**], the latter of which is prerequisite for a charge density wave transition. The La ions in T phase are octahedrally coordinated, which is known to split the five-fold degeneracy of *d* orbitals into triply degenerate t_{2g} states and doubly degenerate e_g states, with the former lying below the latter [see **Fig. 2(d)**]. The

three-fold t_{2g} states form the three bands near the Fermi level of T $LaBr_2$, which span a wide energy range from around -0.88 eV to 2.67 eV. The $5d^1$ electrons from La partially occupy such wide degenerate bands and are not subject to spin polarization.

The 2×1 CDW distortions in the T'-phase $LaBr_2$ can be understood by the chemical bonding between La ions, leading to a split of t_{2g} orbitals into bonding [t_{2g}(b)], non-bonding [t_{2g}(nb)] and anti-bonding [t_{2g}(ab)] states, as shown in **Figs. 2(b)** and **(d)**~~. A similar mechanism has been proposed for the T' phase TMDs but with important differences. [17]).~~ The bonding t_{2g} states here are well isolated and are separated by 0.32 eV from the non-bonding states. Such a transition from wide bands to well separated states has also been shown in simple metals by strong compression, leading to the formation of interstitial localized electrons. [43] The isolated bands are a signature of electrides, as the AEs are localized at interstitial sites and hybridize marginally with other states. [36,44] Notably, the constructed Maximally Localized Wannier Functions (MLWFs) for the bonding t_{2g} states indicate a multi-center chemical bonding between the neighboring three La ions, [see **Fig. 4(b)**] in line with the reported mechanism for the formation of ambient-pressure electrides. [38]

Thus, we propose the formation of electride states as the mechanism for the 2×1 CDW distortions in the T'-phase $LaBr_2$. The inapplicability of the fermi surface nesting picture for the CDW in this system is discussed in the Supplemental Material (SM). Further evidences of its electride nature by the projected density of states, band decomposed charge density and electron localization function can also be found in SM. [45] Such a systematic analysis has helped us successfully identify tens of layered electrides from

Materials Project database. [36,46]

To directly show the charge density modulation after the CDW transition in $LaBr_2$, we calculated the partial charge density of the $5d^1$ electrons of La in T-phase and T'-phase, by integrating the states with a same energy window from Fermi level to -1.0 eV. As the planer average partial charge along *b* axis shown in **Fig. 3(a)**, the $5d^1$ electrons of La in T-phase $LaBr_2$ are somewhat uniformly distributed with peaks around the La atoms, in line with its distribution in the three-dimensional (3D) visualization in **Fig. 3(b)** and the large bandwidth in **Fig. 2(a)**. With the 2×1 CDW distortions, the profile of planer average charge density changes significantly. The La $5d^1$ electrons are more localized in the T'-phase $LaBr_2$ and the peaks of charge density locate at the interstitial region between the dimerized La atoms, which is further supported by the 3D visualization in **Fig. 3(d)** and the small bandwidth in **Fig. 2(c)**. As the partial charge in a higher isosurface value of 8×10^{-3} $e^-/$ $Å^3$ shown in **Fig. S2(b)**, it is noticeable that the $5d^1$ electrons locate mainly at the interstitial sites as anionic electrons in T'-phase $LaBr_2$. These results clearly demonstrate the formation of anionic electrons as the charge density modulation for the CDW transition in T-phase $LaBr_2$. As a direct comparison, the partial charge of the Mo d^2 electrons in T' MoS_2 is also simulated, which shows peaks at the Mo positions and the absence of anionic electrons (see SM **Fig. S4**).

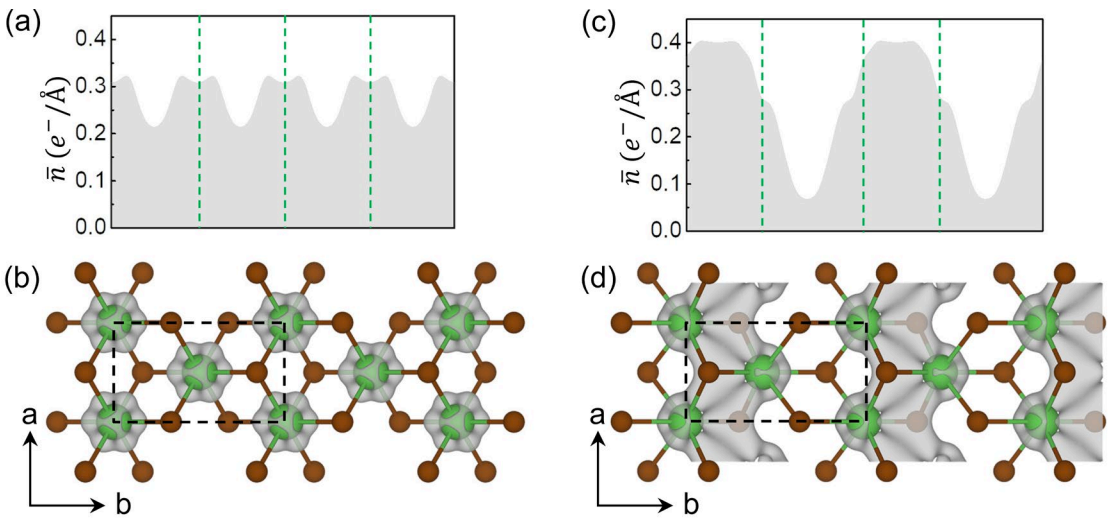

FIG. 3. Partial charge density for the La d^1 electrons (a) by planer average along b axis and (b) by 3D visualization in grey (isosurface value = 6×10^{-3} e$^-$/ Å^3) for T-phase $LaBr_2$. (c) and (d) are same as (a) and (b) but for T' $LaBr_2$. The green vertical dash lines in (a) and (c) indicate the corresponding positions of La ions in (b) and (d), respectively.

In the following, we further study the magnetic properties of T'-phase $LaBr_2$. As shown in **Fig. 2(b)**, the two La $5d^1$ electrons of the dimerized La ions lead to half-filled bonding t_{2g} bands. Interestingly, the bonding t_{2g} bands are more localized with a reduced band width of around 0.93 eV and correspondingly increased density of states at the Fermi level (see more details in **Fig. S6**), causing electronic instability to the system. The electronic structure of T' $LaBr_2$ calculated with the spin polarization [**Fig. 2(c)**] shows a full spin-splitting of the anionic electron bands (1 μ_B per La atom), leading to a Mott insulating state with a band gap of around 0.65 eV [calculated by hybrid functional (HSE06)]. It is noted the band gap opening of T' $LaBr_2$ is only obtained by the hybrid functional simulations and it remains to be metallic under pure GGA calculations, which demonstrate the correlation nature of the anionic electrons.

The schematic energy level diagrams shown in **Fig. 2(d)** summarize the transition process from the nonmagnetic metallic T phase to the magnetic Mott insulating T' $LaBr_2$.

As the spin density of the T'-$LaBr_2$ shown in **Figs. 4 (a)**, the main contribution to the magnetic moments is from the two atomic-orbital-free AEs per unit cell at the interstitial sites between the dimerized La atoms. The dimerized distribution of La atoms leads to a quasi-one-dimensional (1D) magnetic AE stripes. Due to the CDW distortions, the dimerized La atoms are not in the same plane along *c* axis and accordingly the two magnetic AEs have different height as shown in **Fig. 4 (a)**.

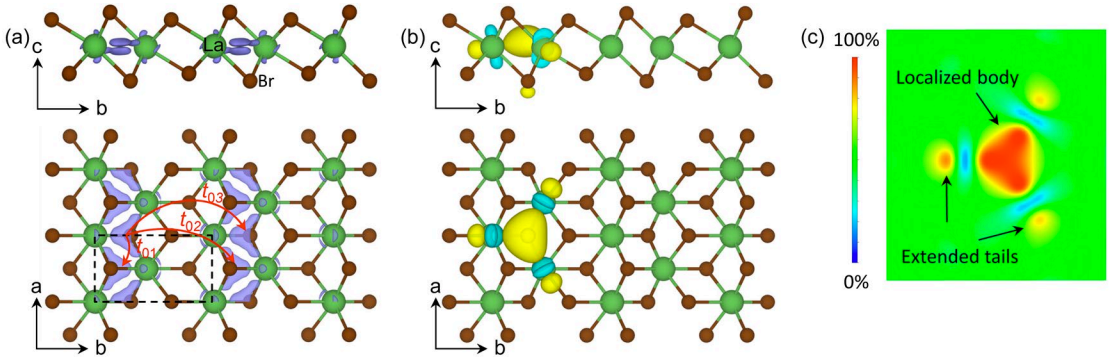

FIG. 4. (a) The spin density (isosurface value = 9.6×10^{-3} $e^-/Å^3$) in purple and (b) the MLWF in yellow and light blue for T' $LaBr_2$. The red arrows in (a) are the schematic representation of the hopping paths between the magnetic anionic electrons. The isovalue of MLWF is set to 5.0. (c) The colored contour plot of MLWF in the plane passing through the La atoms of the magnetic anionic electron state of T' $LaBr_2$. The localized *s*-symmetric body and its extended tails of MLWF are indicated by black arrows.

The atomic-orbital-free magnetic anionic electrons possess a unique dual localized and extended nature as well as a direct exchange coupling from the overlap of the wave functions, which has been reported in non-distorted H-phase $LaBr_2$ monolayer. [35] Similar properties would be expected for the magnetic anionic electrons in CDW distorted $LaBr_2$. It is noted that Coulomb interaction on the non-atomic interstitial sites and their nonlocal direct exchange cannot be fully captured by conventional density functional theory simulations. Thus, we adopt a low-energy effective model for the two anionic electron bands near Fermi level, in which the Hamiltonian of the system based

on the second quantization is given by

$$\widetilde{H} = \sum_{ij} t_{ij}\hat{a}_i^{\dagger}\hat{a}_j + \frac{1}{2}\sum_{i} U_{ii}\hat{a}_i^{\dagger}\hat{a}_i^{\dagger}\hat{a}_i\hat{a}_i + \frac{1}{2}\sum_{ij} U_{ij}\hat{a}_i^{\dagger}\hat{a}_j^{\dagger}\hat{a}_j\hat{a}_i + \frac{1}{2}\sum_{ij} J_{ij}^{D}\hat{a}_i^{\dagger}\hat{a}_j^{\dagger}\hat{a}_i\hat{a}_j \quad (1)$$

where $i(j)$, $\hat{a}_i$ ($\hat{a}_i^{\dagger}$), t_{ij}, U_{ii}, U_{ij} and J_{ij}^{D} are site indices, creation (annihilation) operators, hopping parameters, on-site Coulomb, off-site Coulomb, and off-site direct-exchange interactions, respectively. The parameters in this model can be mapped by the constrained random phase approximation (cRPA) as implemented in VASP, based on maximally localized Wannier functions (MLWFs) using the Wannier90 package. [47] Interstitial *s* orbitals were used as initial guess to construct MLWFs for the anionic electron states. [35] The converged MLWF is visualized in **Fig. 4(b)** and its colored contour plot in the plane crossing the La atoms is shown in **Fig 4 (c)**, both of which demonstrate that the MLWF captures the dual nature of anionic electron with extended tails around the well localized body.

The interactions up to the third nearest neighboring anionic electrons were taken into consideration, whose hopping paths are indicated by the red arrows shown in **Fig. 4(a)**. The parameters obtained from cRPA are listed in **Table 1**. The localized nature of the anionic electrons leads to a large on-site Coulomb interaction of 2.14 eV. The off-site Coulomb interactions are U_{01} = 1.53 eV, U_{02} = 0.87 eV, and U_{03} = 0.84 eV, respectively. The comparable Coulomb interactions between the on-site and off-site (up to a distance of 7.43 Å) interactions are a result of the weak screening from other bands to the well isolated anionic electron bands [see **Fig. 2(b)**]. The extended nature of the aniconic electrons is reflected by the significant off-site direct exchanges of J_{02}^{D} = 1.57

meV and J_{03}^{D} = 1.29 meV at a distance of 6.50 Å and 7.43 Å, respectively, which are beyond the spatial limit of atomic-orbital overlap in conventional direct-exchange systems. These results suggest our proposed magnetic mechanism for magnetic anionic electrons is general for magnetic electrides. [35] Compared with the nearest off-site parameters of H-phase $LaBr_2$ (t_{01} = 12.50 meV, J_{01}^{D} = 21.9 meV) [35], the ones of T' phase (t_{01} = 126.45 meV, J_{01}^{D} = 53.80 meV) are considerably larger. This can be understood by the facts that T' $LaBr_2$ has shorter nearest neighboring sites (2.41 Å vs. 4.14 Å) and a larger bandwidth of the anionic electron bands (0.93 eV vs. 0.50 eV) than that of H phase.

Table 1. Calculated parameters of the low-energy effective model for T' $LaBr_2$. The hopping paths are shown in Fig. 4(a). d_{ij} is the distance of the hopping path. The on-site Coulomb interaction U_{00} is 2.14 eV.

path	d_{ij} (Å)	U_{ij} (eV)	J_{ij}^{D} (meV)	t_{ij} (meV)	J_{ij} (meV)
0-1	2.60	1.53	53.80	126.45	-1.58
0-2	6.57	0.87	1.57	42.25	1.25
0-3	7.43	0.84	1.29	25.91	-0.26

In the limit $U_{00} > U_{ij} \gg t_{ij}$, the Anderson's model can be applied to determine the overall isotropic exchange interactions of T' $LaBr_2$ as follows.

$$J_{ij} = \frac{2t_{ij}}{\widetilde{U}_{ij}} - J_{ij}^{D} \quad (2)$$

where $\widetilde{U}_{ij} = U_{00} - U_{ij}$ is the effective Coulomb interaction, the first term is the antiferromagnetic (AFM) kinetic superexchange from direct hopping between magnetic centers and the second term is the ferromagnetic (FM) direct exchange from the overlap

of the wave functions of magnetic moments. Using the parameters shown in **Table 1**, we conclude the isotropic magnetic exchange in T' $LaBr_2$ is FM between the AEs within the 1D-like strip, while it is more likely to be AFM between the 1D-like strips from the stronger AFM J_{02} than FM J_{03}.

In summary, via first-principles calculations, we have shown that the T-phase $LaBr_2$ is subject to a structural instability to a 2×1 CDW. Interestingly, the CDW distorted $LaBr_2$ possesses an unexpected magnetic electride state, which is the first report of the formation of interstitial anionic electrons as the CDW charge density modulation to the best of our knowledge. By a combined low energy model, cRPA and Anderson's model, the anionic electron states in T' $LaBr_2$ have been shown to have dual localized and extended nature, leading to an unconventional magnetism, coexisting with CDW. This exotic system may provide an exciting platform to explore new physics and application to the fields of 2D spintronics, CDW, tunable electride, and phase transition.

Acknowledgements

This work is supported by the Ministry of Education, Singapore, under its MOE Tier 1 Awards R-144-000-441-114 & R-144-000-413-114. M.Y. acknowledges the funding support (project ID: 1-BE47) from The Hong Kong Polytechnic University. We acknowledge the computational resources supported by the National Supercomputing Centre (NSCC) Singapore and Centre of Advanced 2D Materials (CA2DM) HPC infrastructure.

References

[1] G. Grüner, Rev. Mod. Phys. **60**, 1129 (1988).

[2] X. Qian, J. Liu, L. Fu2, and J. Li, Science **346**, 1344 (2014).

[3] H. Kim, J. H. Shim, S. Kim, J. H. Park, K. Kim, and B. I. Min, Phys Rev Lett **125**, 157001 (2020).

[4] A. F. Kusmartseva, B. Sipos, H. Berger, L. Forro, and E. Tutis, Phys. Rev. Lett. **103**, 236401 (2009).

[5] C. Chen, B. Singh, H. Lin, and V. M. Pereira, Phys. Rev. Lett. **121**, 226602 (2018).

[6] K. K. Kolincio, M. Roman, and T. Klimczuk, Phys Rev Lett **125**, 176601 (2020).

[7] E. C. Stoner, Proceedings of the Royal Society of London. Series A. Mathematical and Physical Sciences **165**, 372 (1938).

[8] G. Duvjir *et al.*, Nano Lett **18**, 5432 (2018).

[9] P. M. Coelho, K. Nguyen Cong, M. Bonilla, S. Kolekar, M.-H. Phan, J. Avila, M. C. Asensio, I. I. Oleynik, and M. Batzill, The Journal of Physical Chemistry C **123**, 14089 (2019).

[10] A. O. Fumega *et al.*, The Journal of Physical Chemistry C **123**, 27802 (2019).

[11] M. H. Whangbo and E. Canadell, J. Am. Chem. Soc. **114**, 9587 (1992).

[12] S. Manzeli, D. Ovchinnikov, D. Pasquier, O. V. Yazyev, and A. Kis, Nature Reviews Materials **2** (2017).

[13] V. N. Strocov *et al.*, Physical review letters **109**, 086401 (2012).

[14] J. G. Si, W. J. Lu, H. Y. Wu, H. Y. Lv, X. Liang, Q. J. Li, and Y. P. Sun, Physical Review B **101** (2020).

[15] K. Zhang, C. Si, C.-S. Lian, J. Zhou, and Z. Sun, Journal of Materials Chemistry C **8**, 9742 (2020).

[16] L. J. Li, E. C. O'Farrell, K. P. Loh, G. Eda, B. Ozyilmaz, and A. H. Castro Neto, Nature **529**, 185 (2016).

[17] D. Pasquier and O. V. Yazyev, Physical Review B **100** (2019).

[18] K. Rossnagel, Journal of Physics: Condensed Matter **23**, 213001 (2011).

[19] S. Qiao *et al.*, Physical Review X **7** (2017).

[20] D. H. Keum *et al.*, Nature Physics **11**, 482 (2015).

[21] J. L. Dye, Science **301**, 607 (2003).

[22] Y. Zhang, B. Wang, Z. Xiao, Y. Lu, T. Kamiya, Y. Uwatoko, H. Kageyama, and H. Hosono, npj Quantum Mater. **2**, 45 (2017).

[23] Z. Liu, G. Zhao, B. Liu, Z. F. Wang, J. Yang, and F. Liu, Phys. Rev. Lett. **121**, 246401 (2018).

[24] C. Park, S. W. Kim, and M. Yoon, Phys. Rev. Lett. **120**, 026401 (2018).

[25] J. Wang, X. Sui, S. Gao, W. Duan, F. Liu, and B. Huang, Phys. Rev. Lett. **123** (2019).

[26] T. Yu, M. Hirayama, J. A. Flores-Livas, M.-T. Huebsch, T. Nomoto, and R. Arita, Physical Review Materials **5** (2021).

[27] X. Sui, J. Wang, C. Yam, and B. Huang, Nano Lett **21**, 3813 (2021).

[28] H. Tamatsukuri *et al.*, Physical Review B **102** (2020).

[29] T. Inoshita, N. Hamada, and H. Hosono, Physical Review B **92** (2015).

[30] D. L. Druffel, A. H. Woomer, K. L. Kuntz, J. T. Pawlik, and S. C. Warren, Journal

of Materials Chemistry C **5**, 11196 (2017).

[31] J. S. Oh *et al.*, J Am Chem Soc **138**, 2496 (2016).

[32] W. Li, Y. You, and J.-H. Choi, The Journal of Physical Chemistry C **124**, 25316 (2020).

[33] X. Yang, K. Parrish, Y.-L. Li, B. Sa, H. Zhan, and Q. Zhu, Physical Review B **103** (2021).

[34] S. Bae *et al.*, Advanced Functional Materials **31**, 2100009 (2021).

[35] J. Zhou, Y. P. Feng, and L. Shen, Physical Review B **102** (2020).

[36] J. Zhou, L. Shen, M. Yang, H. Cheng, W. Kong, and Y. P. Feng, Chemistry of Materials **31**, 1860 (2019).

[37] J. Zhou *et al.*, Sci Data **6**, 86 (2019).

[38] X. Dong and A. R. Oganov, in *Correlations in Condensed Matter under Extreme Conditions: A tribute to Renato Pucci on the occasion of his 70th birthday*, edited by G. G. N. Angilella, and A. La Magna (Springer International Publishing, Cham, 2017), pp. 69.

[39] M. S. Miao and R. Hoffmann, Acc Chem Res **47**, 1311 (2014).

[40] M. S. Miao and R. Hoffmann, J Am Chem Soc **137**, 3631 (2015).

[41] K. Momma and F. Izumi, J. Appl. Crystallogr. **44**, 1272 (2011).

[42] A. Togo and I. Tanaka, Scripta Materialia **108**, 1 (2015).

[43] B. Rousseau and N. W. Ashcroft, Phys Rev Lett **101**, 046407 (2008).

[44] T. Tada, S. Takemoto, S. Matsuishi, and H. Hosono, Inorg Chem **53**, 10347 (2014).

[45] See Supplemental Material for details of computational methodologies and more

DFT results.

[46] A. Jain *et al.*, APL Materials **1**, 011002 (2013).

[47] A. A. Mostofi, J. R. Yates, Y.-S. Lee, I. Souza, D. Vanderbilt, and N. Marzari, Computer Physics Communications **178**, 685 (2008).